PVP - Vol. 64

Fluid Transients and Fluid - Structure Interaction

PVP - Vol. 64

Fluid Transients and Fluid-Structure Interaction

presented at

THE PRESSURE VESSEL AND PIPING CONFERENCE
ORLANDO, FLORIDA
JUNE 27 – July 2, 1982

sponsored by

THE OPERATIONS, APPLICATIONS AND COMPONENTS COMMITTEE
PRESSURE VESSEL AND PIPING DIVISION, ASME

edited by

Y. W. SHIN
ARGONNE NATIONAL LABORATORY
ARGONNE, ILLINOIS

F. J. MOODY
GENERAL ELECTRIC COMPANY
SAN JOSE, CALIFORNIA

M. K. AU-YANG
BABCOCK & WILCOX COMPANY
LYNCHBURG, VIRGINIA

THE AMERICAN SOCIETY OF MECHANICAL ENGINEERS
United Engineering Center 345 East 47th Street New York, N. Y. 10017

Library of Congress Catalog Card Number 82-71618

FOREWORD

Fluid transients, structural response, and their interaction are important subjects of study in the design and safe operation of power plants. Fluid transients produce forces that induce structural responses. When the structural displacement is small, these fluid forces may be considered to be decoupled from the structural response, which can then be computed taking into account the effect of fluid-structure interaction by what is commonly called the weak coupling scheme. When the structural displacement is large, however, the feedback effects on the fluid forces can be significant, and the equations of fluid and structural dynamics must then be considered simultaneously. Steady advances have been made in recent years in this relatively new and difficult subject of fluid-structure interaction. Yet, new requirements and challenges continue to evolve, often prompted by economic and safety considerations, particularly in the nuclear power industry.

This symposium, which is sponsored by the Operations, Applications, and Components Committee of the Pressure Vessel and Piping Division, aims at providing a forum for bringing together recent advances in the state of the art of the subject area, with emphasis on flow transients and large structural response. Readers may be interested in earlier publications from ASME symposia on the same or related subjects: "Fluid-Structure Interactions Phenomena in Pressure Vessel and Piping Systems," edited by M. K. Au-Yang and S. J. Brown (ASME Special Publication PVP-PB-026, 1977); "Fluid Transients and Acoutics in the Power Industry," edited by C. Papadakis and H. Scarton (ASME Special Publication, 1978); "Dynamics of Fluid-Structure Systems in the Energy Industry," edited by M. K. Au-Yang and S. J. Brown (PVP-39, 1979); "Interactive Fluid-Structural Dynamic Problems in Power Engineering," edited by M. K. Au-Yang and F. J. Moody (ASME Special Publication PVP-46, 1981); "Fluid Transients and Structural Interactions in Piping Systems," edited by P. H. Rothe and D. C. Wiggert (ASME Special Publication, 1981).

Technical challenges presented by the transient response of fluids or structures or combined fluid-structure systems fall into three categories: observation, formulation, and interpretation. Some papers in this volume emphasize observation, which involves experimental studies of a phenomenon to help understand it better. Some papers emphasize formulation of phenomena, which involves a development of the governing equations with all the essential physics. And some papers emphasize interpretation, which may involve solving the governing equations analytically or numerically or extracting and displaying results in a way that conveys useful information.

This symposium publication is basic enough for use by entry-level workers, but yet has the breadth and depth required by experienced contributors who are working at the state of the art. It is divided into three parts:

Internal flows and transients, which includes fluid transients in various geometries.

Fluid and piping systems, which includes unsteady flow in both flexible and rigid piping systems.

Fluid/structure interaction, which includes new insights into the coupled response of fluid-structure systems.

Our objective in editing this volume was to select papers that present new information and ideas in fluid-structural dynamics. We tried to avoid too much overlap with work reported earlier. Some papers in this volume raise new questions, and some may be controversial. We evaluated the reviewers' comments for each paper and selected those which, in our judgment, would be most useful to the majority of workers in this developing field.

The symposium organizers gratefully acknowledge the work of the contributing authors; we also appreciate the valuable time spent in evaluation of the papers by the reviewers.

Y. S. Shin
Argonne National Laboratory

F. J. Moody
General Electric Company

M. K. Au-Yang
The Babcock & Wilcox Company

CONTENTS

FLUID-STRUCTURAL DYNAMICS I – INTERNAL FLOWS AND TRANSIENTS

Hydrodynamics of Annular-Dispersed Flow
M. Ishii and I. Kataoka 1

Fluid Transients in Two Spatial Dimensions
E. B. Wylie 19

Acoustic Response of a Rectangular Fluid Region by the Method of Images
W. H. Cheng, K. Karim-Panahi and J. R. Fitch 32

WHAMMOCII – A Computer Code for Performing One or Two Phase Water-hammer Analysis
W. J. Krotiuk 44

Acoustic Pressure Field Near the Junction of a Circular Vent and a Rectangular Pool
K. Karim-Panahi and W. H. Cheng. 63

Unsteady Flow Approximation for Low Quality Steam Water Mixtures
D. Katze 71

An Alternative Viscosity Term in the Governing Equation of Coupled Fluid-Structure Wave Motions
K. Karim-Panahi 85

Simulation of Thermal Transient Induced Pipe Flow Stratification Using Commix-2
V. L. Shah, H. M. Domanus, C. C. Miao, R. C. Schmitt, and W. T. Sha. . . . 91

FLUID-STRUCTURE DYANMICS II – FLUID AND PIPING SYSTEMS

Acoustic Analysis of Liquid-filled Piping by Component Synthesis: Experimental Validation and Examination of Assumptions
F. J. Hatfield, L. C. Davidson, and D. C. Wiggert 106

An Elastic-Plastic Pipe Response Model for Small Thickness to Diameter Ratio Pipes in Waterhammer Analysis
A. H. Wiedermann 116

The Effect of Elbow Translations on Pressure Transient Analysis of Piping Systems
R. S. Otwell 127

Theoretical Analysis of Steam Bubble Collapse, Wave Propagation and Structural Responses for Waterhammer Transients in a Piping Network
W. M. Hurwitz 137

Hydrodynamics and Structural Effects Due to the Feedwater Line Blowdown with Check Valve Slam
A. Rutkowski, H. Y. Chang, S. Lim, and M. Lakis 155

Dynamic Transients Induced by Valve Opening in Steam Lines
M. Mikasinovic and R. Hoy 174

Blazer–A Relap5/Modi Post Processor to Generate Force-time History Input Data for Structural Computer Codes
A. G. Ware and R. L. Williamson 183

Modeling Pressure Pulsation in Piping Systems with an Arbitrary Number of Input and Outputs
Z. Xie, A. G. Doige, and T. Y. Lung 199

FLUID-STRUCTURAL DYNAMICS III – FLUID/STRUCTURE INTERACTION

Thermal Damping Effects in Fluid-Structure Interaction
F. J. Moody 221
Some Aspects of Fluid-Structure Coupling
R. F. Kulak 244
Methods for Simulating Fluid-Structure Interaction and Cavitation with Existing Finite Element Formulations
R. E. Schwirian 261
Fluid/Structure Interaction in Cylindrical Containers
L. J. Stefik, Jr. 286
A Multi-Dimensional Arbitrary Lagrangian-Eulerian Method for Dynamic Fluid-Structure Interaction
C. Y. Wang and W. R. Zeuch 298
An Approximate Finite Element Approach to the Evaluation of Fluid Mass Coupling Effects in Dynamic Analysis of Cylindrical Shell Structures
G. C. Mok 317
Free Vibrations in Gas-Liquid-Structure Systems
F. M. Joos and P. W. Huber 349
Simplified Early Time Approximations for Fluid Structure Interaction Computations
A. S. Kushner 366

HYDRODYNAMICS OF ANNULAR-DISPERSED FLOW

M. Ishii and I. Kataoka*
Reactor Analysis and Safety Division
Argonne National Laboratory
Argonne, Illinois

ABSTRACT

The interfacial drag, droplet entrainment, and droplet size distributions are important for detailed mechanistic modeling of annular dispersed two-phase flow. In view of this, recently developed correlations for these parameters are presented and discussed in this paper. The drag correlations for multiple fluid particle systems have been developed from a similarity hypothesis based on the mixture viscosity model. The results show that the drag coefficient depends on the particle Reynolds number and droplet concentration. The onset of droplet entrainment significantly alters the mechanisms of mass, momentum, and energy transfer between the film and gas core flow as well as the transfer between the two-phase mixture and the wall. By assuming the roll wave entrainment mechanism, the correlations for the amount of entrained droplet as well as for the droplet size distribution have been obtained from a simple model in collaboration with a large number of data. The comparison of the correlations to various data show satisfactory agreement.

NOMENCLATURE

A_i	Interfacial area of a particle
A_d	Projected area of a particle
a_i	Interfacial area per unit volume
B_d	Volume of a particle
C_D	Drag coefficient
D	Droplet diameter
D^*	Dimensionless hydraulic diameter given by Eq. (5)
D_h	Hydraulic diameter
D_{max}	Maximum droplet diameter

*Visiting scientist from Institute of Atomic Energy, Kyoto University, Uji, Kyoto, Japan.

$\bar{D}_{nm}$	Mean droplet diameter defined by Eq. (17)
D_{vm}	Volume median droplet diameter
E	Fraction of liquid flux flowing as droplet (= j_{fe}/j_f)
E_{th}	Theoretical upper limit of E
E_∞	Equilibrium value of E
F_D	Drag force
F_v	Virtual mass force
f(D)	Number density distribution function
g	Acceleration due to gravity
j_f	Volumetric flux of total liquid (superficial velocity)
j_{ff}	Volumetric flux of liquid film
j_{fe}	Volumetric flux of droplets
j_g	Volumetric flux of gas
j_g^*	Dimensionless gas flux given by Eq. (3)
M_{id}	Interfacial force for a dispersed phase
M_{ik}	Interfacial force for k phase
m	Exponent
N_d	Number density of dispersed phase
N_μ	Viscosity number
n	Exponent
p_k	Pressure of k phase
Re_f	Total liquid Reynolds number defined by Eq. (4)
Re_{ff}	Film Reynolds number defined by Eq. (10)
Re_g	Gas Reynolds number (= $\rho_g j_g D_h/\mu_g$)
r_d	Particle radius
r_{sm}	Sauter mean radius
t	Time
v_c	Velocity of continuous phase
v_d	Velocity of dispersed phase
v_{ik}	Interfacial velocity
v_k	Velocity of k phase
v_r	Relative velocity

W_f Total liquid mass flow rate

W_{fe} Droplet mass flow rate

We Weber number for entrainment defined by Eq. (8)

y Parameter defined by Eq. (16)

z Axial distance from inlet

Greek Symbols

α_d Void fraction of dispersed phase

α_k Void fraction of k phase

Γ_k Mass source of k phase

Δ Volume fraction oversize

ζ Dimensionless distance

μ_f Viscosity of liquid

μ_g Viscosity of gas

μ_m Mixture viscosity

ξ Parameter in Eq. (21)

$\Delta\rho$ Density difference

ρ_c Density of continuous phase

ρ_g Density of gas

ρ_f Density of liquid

ρ_k Density of k phase

σ Surface tension

$\bar{\tau}_k$ Average viscous stress for k phase

τ_k^t Turbulent stress for k phase

τ_i Interfacial shear stress

INTRODUCTION

In predicting two-phase flow transients, the interfacial transfer terms are among the most essential factors in the modeling. The interfacial transfer terms in a two-fluid model specify the rate of mass transfer, momentum exchange, and heat transfer at the interface between phases. In annular two-phase flow, the droplet entrainment from a liquid film by a streaming vapor core flow is of considerable practical importance for heat and mass transfer processes. The onset of droplet entrainment significantly alters the mechanisms of mass, momentum, and energy transfer between the liquid film and core flow as well as the transfer between the mixture and the wall.

In order to accurately predict a number of important physical phenomena in annular-dispersed flow and in a post-dryout regime, an understanding of the mechanisms of the entrainment and accurate correlations for the onset of entrainment and amount of entrainment are essential. Furthermore, the drag correlation for a

multiparticle system and a droplet size or size distribution are important in determining the heat and momentum transfer between the droplets and vapor. In particular, the dryout and post-dryout heat fluxes (1-3) and the effectiveness of the emergency core cooling systems in light water reactors (4, 5) are significantly affected by the amount and size of droplets which can be entrained in vapor. However, the usefulness of accurate correlations for entrainment, drag force and droplet size are not limited to these special cases mentioned above. General thermohydraulic predictions in annular two-phase flow can be significantly improved by a reliable method of calculating these parameters. In view of their essential importance for the two-fluid model formulations (6-13), which are based on two sets of conservation equations of mass, momentum and energy of each phase, the constitutive relations for droplet entrainment, drag coefficient and droplet size are discussed in detail and practical correlations are recommended in this paper.

ENTRAINMENT

In a system where a liquid film flow along the wall with a gas phase flowing over it, several hydrodynamic transitions leading to entrainment of some of the liquid as droplets are possible (14-16). At certain relative velocity interfacial waves appear and as the relative velocity is increased these dynamic waves can transform to large amplitude roll waves which propagate in one direction. At the roll wave transition or at a slightly higher gas velocity, the onset of entrainment has been observed. Detailed reviews of experimental and analytical work on the inception of liquid entrainment have been presented by Zuber (17), Wallis (18), Hewitt and Hall-Taylor (15), Kutateladze (19), and Ishii and Grolmes (20).

There are several different entrainment mechanisms (15, 20), and it has been observed that the onset of entrainment can depend on the flow directions. By considering these possibilities detailed criteria for onset of entrainment have been developed (20). For the annular flow of low viscous fluids such as water or sodium, the entrainment mechanism based on the shearing-off of roll wave crests is the predominant mode (see Fig. 1). The onset of entrainment occurs when the retaining force of surface tension is exceeded by the interfacial shear force exerted by the streaming gas flow. This inception criterion is given in a non-dimensional form by

$$\frac{\mu_f j_g}{\sigma}\sqrt{\frac{\rho_g}{\rho_f}} \geq 11.78\, N_\mu^{0.8}\, Re_f^{-1/3} \qquad (1)$$

where the viscosity number is given by $N_\mu \equiv \mu_f/(\rho_f \sigma \sqrt{\sigma/g\Delta\rho})^{1/2}$ and the liquid Reynolds number by $Re_f = \rho_f j_f D_h/\mu_f$. Furthermore, there is a rough turbulent regime where the critical gas velocity is independent of the liquid Reynolds number. This regime occurs for $Re_f > 1635$.

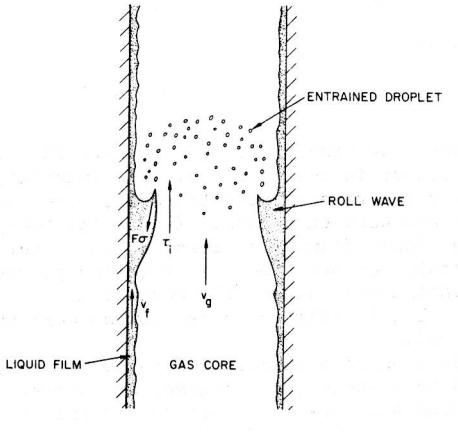

Fig. 1 Roll Wave Entrainment Mechanism

The above criterion is compared to experimental data in Fig. 2. Although there are considerable scattering of data around the criterion, mainly due to different techniques used for different data and also due to the inclusion of data for highly viscous fluids, the overall trend is well predicted.

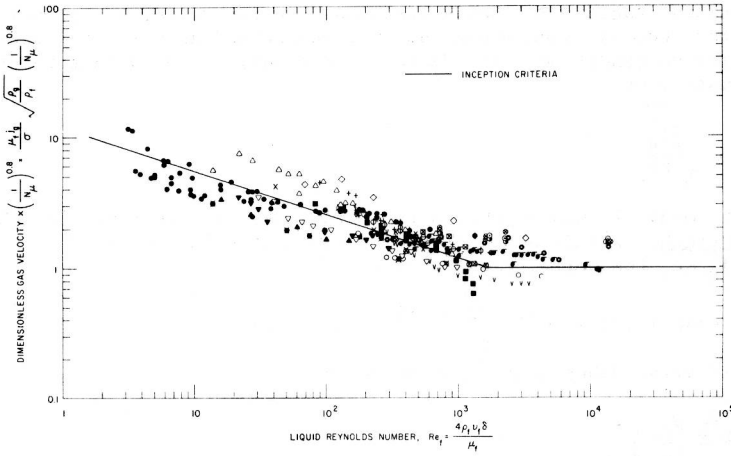

Fig. 2 Onset of Entrainment Criterion Based on Shearing-off of Roll Wave Crests by Ishii and Grolmes (20)

The important parameter concerning the entrainment is the amount of liquid flowing as droplets. This can be considered in terms of the fraction of liquid flux entrained which is defined by

$$E \equiv \frac{W_{fe}}{W_f} = \frac{j_{fe}}{j_f} \tag{2}$$

where W_{fe}, W_f, j_{fe} and j_f are droplet mass flow rate, total liquid mass flow rate, droplet volumetric flux, and total liquid volumetric flux, respectively. Paleev and Filipovich (21), Wallis (22), and Wicks and Dukler (23) have presented correlations based on experimental data.

Recently a more accurate correlation (24) has been proposed based on a simple model and a number of experimental data. The model is obtained by considering the mechanism of shearing-off of roll wave crests by streaming gas flow. First, starting from a force balance for the onset of entrainment, the theoretical limit of entrainment E_{th} is calculated from Eq. (1). This limit is obtained by assuming that the excess liquid beyond the onset of entrainment is completely entrained. Thus the film Reynolds number satisfies Eq. (1) rather than the total liquid Reynolds number. It is expected that this limit E_{th} is much larger than the actual fraction of entrainment, E. However, proper dimensionless parameters can be obtained from this limit.

Furthermore, by considering the effect of increased inertia of gas core flow due to the existence of droplets and the effect of droplet deposition, basic dimensionless parameters have been identified. It has been found that the fully developed entrainment depends on three dimensionless groups given by

Dimensionless Gas Flux

$$j_g^* = \frac{j_g}{\left[\frac{\sigma g \Delta\rho}{\rho_g^2}\left(\frac{\rho_g}{\Delta\rho}\right)^{2/3}\right]^{1/4}} \tag{3}$$

Total Liquid Reynolds Number $$Re_f = \frac{\rho_f j_f D_h}{\mu_f} \quad (4)$$

Dimensionless Diameter $$D^* = D_h \sqrt{\frac{g\Delta\rho}{\sigma}} \quad . \quad (5)$$

The entrained fraction reaches a quasi-equilibrium value, E_∞, at points far removed from the tube entrance where the entrainment and deposition processes attain an equilibrium condition. The distance necessary to reach this condition is given approximately by

$$z \simeq 600\, D_h \sqrt{\frac{j_g^*}{Re_f}} \quad (6)$$

for cases with smooth liquid injection as a film. At this entrance length the entrainment has reached within about 2% of its ultimate value. Then for the region $z \gtrsim 600\, D_h \sqrt{j_g^*/Re_f}$ the correlation becomes

$$E \simeq E_\infty = \tanh\,(7.25 \times 10^{-7}\, j_g^{*2.5}\, D^{*1.25}\, Re_f^{0.25}) \quad . \quad (7)$$

Now an effective Weber number can be defined as

$$W_e \equiv \frac{\rho_g j_g^2 D_h}{\sigma} \left(\frac{\Delta\rho}{\rho_g}\right)^{1/3} \quad (8)$$

where $(\Delta\rho/\rho_g)^{1/3}$ stands for the effect of increased inertia of gas core flow due to droplets. Then the entrainment fraction becomes

$$E_\infty = \tanh\,(7.25 \times 10^{-7}\, W_e^{1.25}\, Re_f^{0.25}) \quad . \quad (9)$$

It is noted that the above expression is given in terms of the Weber number and total liquid Reynolds number. As can be seen here, if the Weber number is used, the significant length scale is D_h. Then the Taylor wavelength scale, $\sqrt{\sigma/g\Delta\rho}$, which is the standard length scale for interfacial phenomena, does not appear in the correlation.

The film Reynolds number Re_{ff} is defined by

$$Re_{ff} \equiv \frac{\rho_f j_{ff} D_h}{\mu_f} \quad (10)$$

where j_{ff} is the liquid film volumetric flux. Thus it satisfies $j_f = j_{ff} + j_{fe}$. Then from definitions

$$Re_{ff} = Re_f(1 - E_\infty) \quad . \quad (11)$$

By substituting Eq. (11) into Eq. (9), the equilibrium entrainment fraction can be resolved in terms of the Weber number and the film Reynolds number. Then it can be shown that

$$E_\infty \doteq 7.75 \times 10^{-7}\, W_e^{1.25}\, Re_{ff}^{0.25} \quad (12)$$

for a wide range of E_∞ from 0 to 0.97. The correlation given by Eq. (7) has been compared to many experimental data for air-water systems in the ranges of $1 < p < 4$ atm, $0.95 < D_h < 3.2$ cm, $370 < Re_f < 6400$, and $j_g < 100$ m/sec, and the result has shown to be satisfactory (see Fig. 3). The various parametric dependencies have been explained in terms of physical mechanisms and information obtained from the onset of entrainment criterion developed previously.

Some experimental data indicated the strong entrance effect as well as the gas expansion effect due to the axial pressure drop in a low pressure system. For the correlation development it was essential to use a local gas velocity or volumetric flux based on a local pressure in evaluating data. By separating these two effects, an additional correlation for the entrance effect on entrainment

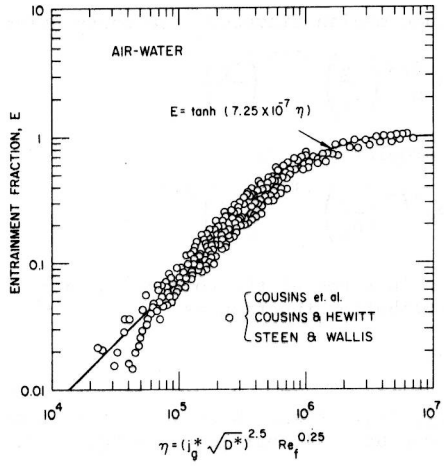

Fig. 3 Comparison of Equilibrium Entrainment Correlation to Various Data

have been developed. As mentioned above, the entrance region is given by $0 < z < 600\ D_h \sqrt{j_g^*/Re_f}$ for cases with smooth liquid film injection. The correlation takes a typical form of an exponential relaxation, and it essentially reaches the quasi-equilibrium value given by E_∞ for large values of z, thus

$$E = \left(1 - e^{-10^{-5}\zeta^2}\right) E_\infty \quad . \tag{13}$$

Here ζ is the dimensionless distance given by

$$\zeta = \frac{z}{D_h}\sqrt{\frac{Re_f}{j_g^*}} \quad .$$

A number of data from the entrance region have been successfully correlated by this expression. This inclusion of entrance effect in the correlation is a significant improvement over the conventional correlations for the entrainment fraction (15, 21-23). From Eq. (13), it can be observed that the fraction of liquid in the entrance region can be significantly smaller than that in the fully developed regime, if the liquid flow starts as a film flow at the entrance. The distance necessary to reach the approximate equilibrium condition is given by Eq. (6). For example, at a typical condition of $j_g^* = 40$ and $Re_f = 3000$, this entrance region is about 70 D_h long.

DROPLET SIZE AND SIZE DISTRIBUTION

The mean droplet size and size distribution are important for detailed mechanistic modeling of annular two-phase flow. A large number of experimental data indicate that the standard Weber number criterion based on the relative velocity between droplets and gas flow predicts far too large droplet sizes. Therefore, it was postulated that the majority of the droplets were generated at the time of entrainment and the size distribution was the direct reflection of the droplet entrainment mechanism based on roll-wave shearing-off. A detailed model of the droplet size in annular flow was then developed based on the above assumption (25). The correlations for the volume mean diameter as well as the size distribution were obtained in collaboration with a large number of experimental data. A comparison with experimental data indicated that indeed the postulated mechanism has been the dominant factor in determining the drop size. Furthermore, a large number of data can be successfully correlated by the present model.

In terms of the volume median diameter, the correlation is given by

$$D_{vm} = 0.0099 \frac{\sigma}{\rho_g j_g^2} Re_g^{2/3} \left(\frac{\rho_g}{\rho_f}\right)^{-1/3} \left(\frac{\mu_g}{\mu_f}\right)^{2/3} . \quad (14)$$

And the average maximum droplet size is

$$D_{max} = 0.031 \frac{\sigma}{\rho_g j_g^2} Re_g^{2/3} \left(\frac{\rho_g}{\rho_f}\right)^{-1/3} \left(\frac{\mu_g}{\mu_f}\right)^{2/3} . \quad (15)$$

The distribution is given in terms of the volume fraction over size Δ and the upper limit log-normal distribution function as

$$\frac{d\Delta}{dy} = - \frac{0.884}{\sqrt{\pi}} e^{-0.781y^2} \quad (16)$$

where $y = \ln [2.13\ D/(D_{max}-D)]$. Figure 4 shows that a large number of data on drop size distributions can be well correlated by Eq. (16).

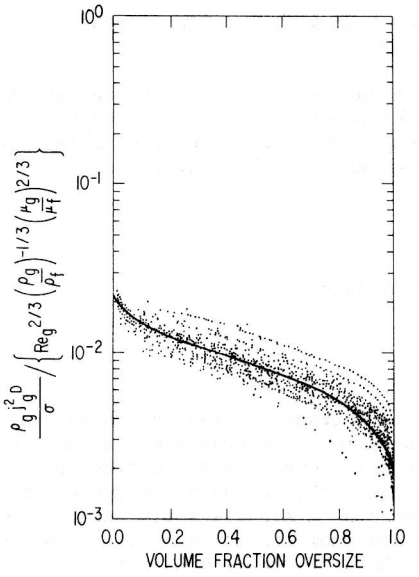

Fig. 4 Droplet Size Distributions in Nondimensional Droplet Diameter vs. Volume Fraction Oversize Plot for Data of Wicks and Dukler (28, 29), Cousins and Hewitt (30), and Lindsted et al. (31)

The above correlation for the droplet size distribution implies that the distribution can be uniquely determined by knowing the volume median diameter. Equation (14) shows that the median diameter is a function of the gas and liquid fluxes. It is noted that this correlation has been developed by considering the hydrodynamic effects only. In a condensing or evaporating system, drop sizes can change due to phase changes. However, the coalescences or disintegrations of droplets should not play a major roll in annular-dispersed flow due to the relatively small sizes of these droplets.

The droplet size distribution predicted by the present correlation indicates the existence of a large number of very small droplets. These droplets are much smaller than the size predicted by the standard Weber number criterion based on the relative velocity between the droplet and vapor. This result has a significant implication in terms of the vapor superheat and post-dryout heat transfer. A number of small droplets give large interfacial area between the liquid and

vapor phases. Therefore, the thermal nonequilibrium should not be very significant. In such cases, these small droplets act as a heat sink due to evaporation, hence it tends to increase the post-dryout heat transfer.

Depending on the transfer mechanisms, several different weighed mean diameters are important for practical applications. By knowing the size distribution, the generalized weighted mean diameter defined below can be calculated.

$$\bar{D}_{nm} = \left[\frac{\int_o^{D_{max}} D^n f(D)\,dD}{\int_o^{D_{max}} D^m f(D)\,dD} \right]^{\frac{1}{n-m}} \tag{17}$$

where f(D) is a number density distribution function and related to the volume oversize function as follows

$$f(D) = \frac{\frac{1}{D^3}\frac{d\Delta}{dD}}{\int_o^{D_{max}} \frac{1}{D^3}\frac{d\Delta}{dD}\,dD} \quad . \tag{18}$$

The calculated ratio of various mean diameters and D_{vm} or D_{max} are listed in Table 1.

Table 1. Various Mean Diameters

Mean Diameter \ Ratio	Mean Diameter / D_{vm}	Mean Diameter / D_{max}
Linear Mean Diameter $\bar{D}_{10}$	0.313	0.100
Surface Mean Diameter $\bar{D}_{20}$	0.409	0.131
Volume Mean Diameter $\bar{D}_{30}$	0.510	0.163
Sauter Mean Diameter $\bar{D}_{32}$	0.796	0.254
Volume Median Diameter D_{vm}	1	0.320

DRAG COEFFICIENT FOR DISPERSED FLOW

The relative velocity between the vapor core flow and droplets is determined by the interfacial drag force. The phase momentum equation of the two-fluid model in a 3-dimensional form (6, 26) is given by

$$\frac{\partial \alpha_k \rho_k \vec{v}_k}{\partial t} + \nabla \cdot (\alpha_k \rho_k \vec{v}_k \vec{v}_k) = -\alpha_k \nabla p_k + \nabla \cdot \alpha_k (\bar{\bar{\tau}}_k + \tau_k^t) + \alpha_k \rho_k \vec{g} + \vec{v}_{ki} \Gamma_k + \vec{M}_{ik} - \nabla \alpha_k \cdot \tau_i \quad . \tag{19}$$

Here α_k, ρ_k, $\vec{v}_k$ and p_k are the void fraction, density, mass weighted mean velocity and pressure of k-phase. Whereas Γ_k, $\vec{M}_{ik}$, $\vec{v}_{ik}$ and $\vec{\tau}_i$ are the mass generation, interfacial drag, interfacial velocity and interfacial shear stress, respectively. The conservation of total momentum requires

$$\Sigma \vec{M}_{ik} = 0 \tag{20}$$

which is the average momentum jump condition.

By neglecting the lift force due to rotations of particles and the diffusion force due to concentration gradient, we may model the generalized drag force for a dispersed phase by a simple model (27) such as

$$\vec{M}_{id} = \alpha_d \vec{F}_D/B_d + \alpha_d \vec{F}_v/B_d + \frac{9}{2}\frac{\alpha_d}{r_d}\sqrt{\frac{\rho_c \mu_m}{\pi}} \int_t \frac{D_d}{D\xi}(\vec{v}_c - \vec{v}_d)\frac{d\xi}{\sqrt{t-\xi}} \tag{21}$$

where $\vec{F}_D$, B_d, $\vec{F}_v$ and μ_m are the standard drag force, volume of a typical particle, virtual mass force, and mixture viscosity, respectively. The last term is the Basset force due to the transient development of a boundary layer development. The standard drag acting on the particle under steady-state conditions can be given in terms of the drag coefficient C_D as

$$\vec{F}_D = -\frac{1}{2} C_D \rho_c \vec{v}_r |v_r| A_d \tag{22}$$

where A_d is the projected area of a typical particle and $\vec{v}_r$ is the relative velocity given by $\vec{v}_r = \vec{v}_d - \vec{v}_c$.

In terms of the weighted mean diameter defined by Eq. (17), A_d for spherical droplets becomes

$$A_d = \pi \bar{D}_{20}^2/4 \quad . \tag{23}$$

However, from Eq. (22)

$$\alpha_d \vec{F}_D/B_d = -\left(\alpha_d \frac{A_d}{B_d}\right)\frac{C_D}{2} \rho_c \vec{v}_r |v_r| \quad . \tag{24}$$

By denoting the number density by N_d, one gets

$$\alpha_d = N_d B_d \tag{25}$$

where

$$B_d = \frac{4}{3}\pi\left(\frac{\bar{D}_{30}}{2}\right)^3 \quad . \tag{26}$$

On the other hand, the interfacial area concentration a_i can be given by

$$a_i = N_d A_i \tag{27}$$

where

$$A_i = 4\pi\left(\frac{\bar{D}_{20}}{2}\right)^2 \quad . \tag{28}$$

Therefore, it can be shown that

$$\alpha_d = \frac{a_i}{6}\frac{\bar{D}_{30}^3}{\bar{D}_{20}^2} \quad . \tag{29}$$

However, by definition